

Fast Three-Dimensional Depth-Velocity Model Building Based on Reflection Traveltime Tomography and Pre-stack Time Migrated Images

D. Neklyudov[1(✉)], K. Gadylshin[1], M. Protasov[1], and L. Klimes[2]

[1] Institute of Petroleum Geology and Geophysics, Novosibirsk 630090, Russia
{neklyudovda,gadylshynkg,protasovmi}@ipgg.sbras.ru
[2] Charles University, 121 16, Prague, Czech Republic
klimes@seis.karlov.mff.cuni.cz

Abstract. We present a robust nonlinear traveltime inversion procedure that enables fast iterative 3D depth velocity model reconstruction. It is based on automatic grid reflection traveltime tomography. To obtain input data necessary for inversion (traveltimes of reflected waves), we utilize conventional seismic time processing products such as normal-moveout velocities and a set of time-migrated reflection horizons picked in the final prestack time migration image. Ray-based tomographic inversion fits prestack traveltimes. They are approximated by hyperbolae using the developed effective engine of grid reflection tomography. We prove the effectiveness of the proposed approach numerically using a real-life example.

Keywords: Traveltime tomography · Inverse problem · Time migration · Depth migration · Seismic exploration

1 Introduction

Nowadays, Pre-Stack Depth Migration (PSDM) has become a necessary tool in the practice of seismic data processing. Traditionally, depth migration results are called "depth seismic images" of an area under investigation. PSDM is especially important in areas with complex geological conditions in the presence of strong lateral variations of geological properties. The reliability of depth images depends entirely on the adequacy of the depth-velocity model of the medium in which PSDM is performed. Methods oriented for depth-velocity model building are based on the use of traveltimes of recorded seismic waves. Detailed reviews of existing methods that are widely used in seismic exploration can be found in the books [1–3]. Here we outline one specific feature of reflection traveltime tomography. Obtaining traveltime of reflected waves in practice is difficult (compared with traveltimes of transmitted or refracted waves observed as first arrivals within seismic records). There are two main reasons: 1) amount of seismic data acquired during modern seismic surveys oriented for reflections is enormous. It is about tens (and hundreds) of terabytes; 2) Poor quality of recorded data. Seismic records of reflected

© Springer Nature Switzerland AG 2021
O. Gervasi et al. (Eds.): ICCSA 2021, LNCS 12950, pp. 282–295, 2021.
https://doi.org/10.1007/978-3-030-86960-1_20

waves (seismograms) represent a complex pattern of interfering arrivals of various types of elastic waves. Identification of reflected arrivals, even using preliminarily processed data, is a challenging task. Reflections are difficult to distinguish because they are weak in comparison with residual coherent and random noise. These reasons exclude "manual" picking of reflection traveltimes in the practice of industrial seismic exploration. The challenge is to robustly extract traveltimes of the reflected waves from complex, noisy wavefields in an automated way.

An effective solution is provided by migration velocity analysis (MVA). MVA has now become the standard practical method for depth-velocity model building [4]. The basic idea behind MVA may be described in a simplified form as follows. Suppose some approximate initial depth-velocity model is provided. In that case, PSDM is performed for several common-offset gathers (i.e., specifically chosen subvolumes of the whole seismic dataset) when the offsets range is fixed. The set of calculated depth images corresponding to different offset are ordered into so-called Common Image Gathers (CIG). Each trace of a CIG corresponds to a depth image at a fixed lateral location in the area but obtained using a specific offset (and azimuth). If one considers a certain CIG, it consists of all migrated traces obtained using different offsets but depicting the medium's same area. If PSDM has been done using the "correct" depth-velocity model, then would align images of reflections in the CIG. The natural assumption used here is that the images of the same reflection surface should be at the same depth, regardless of the data parameters (such as offset or azimuth) from which built these images. If the depth-velocity model is incorrect, images of reflective surfaces in the CIG will have a shape different from the straight line. It is called residual moveout (RMO). The RMO analysis performed within the entire volume of the depth seismic image allows for correcting the current depth-velocity model. Each coherent event's curvature in each CIG, which is associated with a reflective surface in-depth, is recalculated into the traveltime residual of the corresponding reflected wave. (Here, the term "traveltime residuals" means the difference of traveltime of the reflected wave in the current and "correct" depth-velocity model).

Estimated reflection traveltime residuals are the input for linear traveltime tomography. As a result of traveltime inversion, a refinement of the depth velocity model is calculated. The corrected velocity model minimizes the traveltime residuals and accordingly reduces the curvature of RMO in the CIGs. The main practical advantages of MVA are: 1) estimation of reflection traveltimes performs automatically after PSDM. PSDM significantly reduces amount of random and coherent noise in the data is because of "optimal" stacking of seismic data; 2) there is no need for extended seismic horizons in the model since images on CIG are presented as a set of independent locally coherent events. Thus, traveltime tomography refines only the velocity structure of the medium. The geometry of reflectors (their shape and positions), as a rule, is not included in the inversion procedure at the early stages of velocity model building. The disadvantage of MVA is the need to repeat computationally expensive and lengthy cycles of 3D PSDM and perform re-picking at every nonlinear iteration of the velocity model update. To converge effectively, MVA requires starting from an adequate and good enough initial velocity model that provides coherent and focused CIGs for residual moveouts' picking. Robust depth-velocity model estimation approaches which may provide adequate initial

guess for standard MVA have been a field of active research in recent years. The main idea behind these methods is to use products of seismic time processing such as time migration velocity [5–14] or wavefront attributes [15–17].

In this work, we propose a simple and relatively cheap algorithm to recover a reliable but simplified velocity model based on hyperbolic approximation of reflection traveltimes. We presume that such a model may be used as an initial model for standard MVA. A proper initial model allows reducing the number of computationally expensive MVA iterations at the early stages of velocity model building. Our approach is based on processing products, which are readily available at the early stages of seismic processing, namely stacking velocities and final processed "time" image provided by prestack-time migration (PSTM). The essence of the proposed approach is a robust scheme of reflection traveltimes approximation having a set of picked time migrated horizons. The advantages of the proposed algorithm are 1) it is fully automatic and based on well-known grid reflection tomography, 2) there is no need for computationally expensive two-point or dynamic raytracing, 3) it may be easily adopted for higher order traveltime approximations, 4) reflection travetimes approximation may be done azimuthally dependent.

The content of the paper is as follows. First, we present the proposed tomographic workflow and describe in more detail each step of the algorithm. We also cover some implementation details of the developed software code. Next, we present a real-life 3D example.

2 Reflection Traveltime Approximation

PSDM is always performed at the latter stages of seismic data processing workflow. In the steps preceding the PSDM, "time-images" of a target area are constructed using pre-stack time migration (PSTM). These images are used for preliminary interpretation. Main reflection horizons are usually picked there. Normal-moveout velocities V_{NMO} and velocities of time migration V_{MIG} are also always available at this stage. It is usually supposed that V_{MIG} approximate the root mean square velocity, V_{RMS}. Having these products of time processing an efficient algorithm for reflection traveltime tomography may be suggested. Below we describe the proposed algorithm in more detail. First, we specify the "ingredients" needed for workflow:

1. Initial depth velocity model. Usually, it is constructed from the available time migration velocities V_{MIG} using the Dix formula [18]. In most cases, even in areas with moderate lateral velocity variations, such a model is barely acceptable and unable to provide a reliable depth image.
2. Main reflection horizons picked in the final PSTM image (in a 3D case, it is a cube), $T^j_{IM}(X_{IM}, Y_{IM})$, j = 1,..N. (N is several horizons.) Each horizon is defined in the form of a table, (X_{IM}, Y_{IM}, T_{IM}), where X_{IM},Y_{IM} are the coordinates at the acquisition surface, T_{IM} is the corresponding image time. Further, we consider each surface as a set of independent locally coherent events. Note that each independent local coherent event is strictly associated with a specific reflection surface.

3. A cube of normal-moveout velocity, $V_{NMO}(X_{CMP}, Y_{CMP}, T_0)$. (Or, optionally, a set of azimuth- dependent cubes, $V_{NMO}(X_{CMP}, Y_{CMP}, T_0; \alpha)$). Here, X_{CMP}, Y_{CMP} are midpoint coordinates, T_0 is two-way traveltime along a normal ray (zero-offset traveltime), α means azimuth on the acquisition surface.

At the first stages of the proposed approach, a "numerical post-stack demigration through depth" of the picked time-migrated reflection surfaces is performed using the concept of "image ray" [19]. This term denotes an auxiliary ray that approaches the acquisition surface along the normal (see Fig. 1). Stages 1–5 described below are performed for each picked time-migrated reflection surface independently.

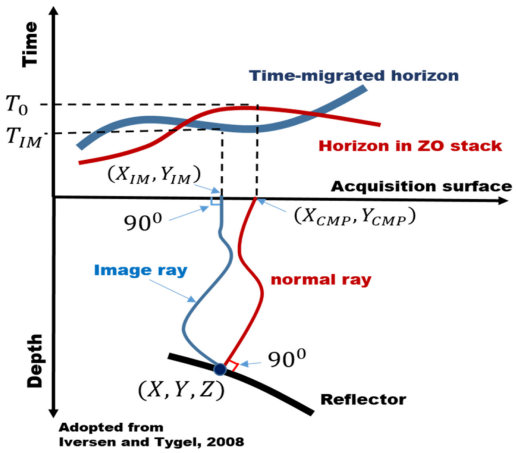

Fig. 1. Image ray and normal ray

1. For each point on the given "time-migrated" surface $T^j_{IM}(X_{IM}, Y_{IM})$, an "image" ray is traced downward within the given initial depth velocity model. It is released from the acquisition surface from the point (X_{IM}, Y_{IM}) along the normal and continues downward until the half image time $T_{IM}/2$ has expired. As a result, the position of the corresponding point (X, Y, Z) in depth is determined. It is repeated for each point of the surfaces T^j_{IM}. As a result, on performs the depth migration (of "time-to-depth conversion") of the "time" reflection horizon using the "image" rays [19]. Each point of the surface T^j_{IM} now has the corresponding position in depth in the current velocity model. The distribution of the points in depth is irregular. Note that the "image" ray provides no information about the local reflection surfaces' normal vector (contrary to normal ray tracing). All that can be said is that the "image" ray touches the reflection surface when the time $T_{IM}/2$ has passed (Fig. 1).
2. At the previous stage, we obtain the distribution of reflection horizon points in depth. Consider a depth point coordinates as a certain function $Z_j(X, Y)$ which is defined as a set of discreet values on a two-dimensional irregular grid (X, Y). It is necessary to determine numerically the surface $Z_j(X, Y)$ normal (Fig. 2). For each

fixed point in depth, its neighbors are collected within some predetermined aperture. A local plane is constructed which is closest to all selected points in the least-squares sense. Thus, the classical three-dimensional linear regression is considered locally. According to the irregular "cloud" of points (X, Y, Z) a set of local reflection surfaces is constructed. It is assumed that each local reflection surface is flat and characterized by its own normal. After time-to-depth conversion by the "image" rays using an incorrect depth-velocity model, initially smooth and regular "time" horizons might become quite irregular in depth. We assume that their local smoothness is preserved. We apply the following procedures: filtration of the values $Z_j(X, Y)$ within the regression, apertures remove outliers; local smoothing of the neighbor normal vectors within a predefined sliding window.

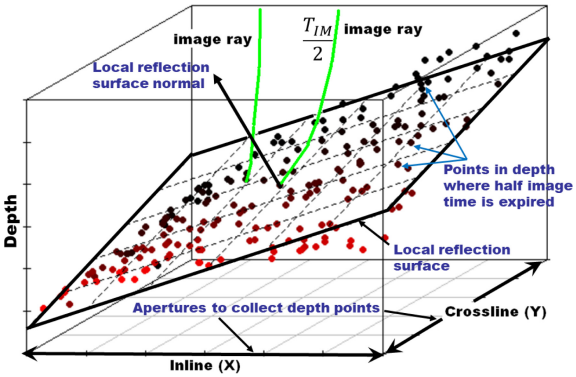

Fig. 2. Local reflection surface normal determination in depth via three-dimensional linear regressions.

3. From each local reflection surface in depth, a normal ray according to surface's normal vector is traced upward toward the acquisition surface. Thus a relation between the time-migrated horizon $T^j_{IM}(X_{IM}, Y_{IM})$ with corresponding zero-offset traveltimes $T^j_0(X_{CMP}, Y_{CMP})$ is numerically constructed. Stages 1–3 are actually "numerical demigration through depth" of "time" migrated horizons picked in the PSTM cube.
4. From each reflection surface with a known normal, a fan of reflected rays is emitted. They are traced upward with certain increments of the opening angles (reflection angles) and azimuths (in depth) (Fig. 3). Each reflected ray consists of two segments satisfying Snell's law at the reflection surface. Let each of the two segments of the reflected ray arrive at the acquisition surface at certain points. These points can be thought of as "virtual" source, and receiver which have their own coordinates (X_S, Y_S) and (X_R, Y_R). Using these coordinates, reflected ray might be uniquely defined by the midpoint coordinates (X_{CMP}, Y_{CMP}), absolute offset h (distance between the source and receiver), and azimuth α. Traveltime $T_{CALC} = T_{CALC}(X_{CMP}, Y_{CMP}, h, \alpha)$ along

each reflected ray is computed in the current depth-velocity model and corresponding elements of tomography matrix, which will be used in traveltime inversion.

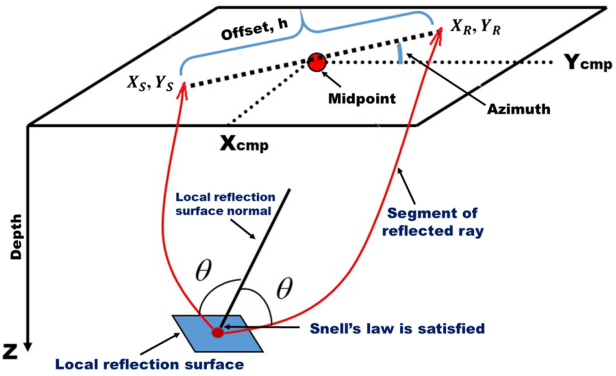

Fig. 3. Calculation of up-going reflected ray emitted from a local reflection surface in depth.

5. "Observed" reflection traveltimes should be determined in each point on the acquisition surface. At this point a reflected ray calculated at stage 4 exists. We suggest approximating actual reflection traveltime using well known 2nd order hyperbolic approximation [20, 21]:

$$T_{\mathrm{OBS}}(X_{\mathrm{CMP}}, Y_{\mathrm{CMP}}, h, \alpha) = \sqrt{T_0^2(X_{\mathrm{CMP}}, Y_{\mathrm{CMP}}) + \frac{h^2}{V_{NMO}^2(X_{\mathrm{CMP}}, Y_{\mathrm{CMP}}, T_0, \alpha)}} \tag{1}$$

Each reflected ray is associated with its midpoint coordinates X_{CMP},Y_{CMP} So it is easy to find the corresponding normal (zero offset) two-way traveltime $T_0 = T_0(X_{CMP}, Y_{CMP})$ (thanks to stage 3) and, therefore, to find the required value $V_{NMO}(X_{CMP}, Y_{CMP}, T_0; \alpha)$. So observed traveltime at a given point may be calculated using expression (1) since all "ingredients" are found. Such approximation is quite robust since V_{NMO} is a very stable parameter. Moreover, NMO velocities are carefully controlled. In principle, it is a purely kinematic parameter, which generally may have nothing in common with the medium's real distribution of interval velocities. Still, it always characterizes the behavior of the reflection traveltimes in the sense of regression. By definition, V_{NMO} characterizes best fits hyperbola that approximate real traveltimes of the reflected waves. More sophisticated approximations may be used here (for example, 4th order approximation described by [22, 23]). Note that NMO velocity may be additionally azimuthally dependent [20]. In that case, "observed" traveltime (1) is calculated, taking into account the reflected ray's azimuth α, i.e., it is necessary to select the NMO velocity corresponding to the given azimuth.

Finally, the input data for standard linear reflection traveltime tomography may be computed. As an input, traveltimes residuals of reflected waves are used:

$$dT(X_{CMP}, Y_{CMP}, h, \alpha) = T_{OBS}(X_{CMP}, Y_{CMP}, h, \alpha) - T_{CALC}(X_{CMP}, Y_{CMP}, h, \alpha) \tag{2}$$

Where T_{CALC} are calculated in stage 4 while T_{OBS} are estimated by expression (1).

6. Linear reflection traveltime tomography using reflection traveltime residuals (2) is performed.

As a result of stage 6, we determine correction to the initial velocity model. After updating of depth velocity model, steps 1–6 of the proposed scheme are repeated in the corrected model. Thus, we perform iterative refinement of the 3D depth-velocity model without involving computationally expensive PSDM procedure. After several global iterations, the velocity model's refinement must be stopped because hyperbolic approximation of reflection traveltimes may be insufficient for reliable reconstruction of the velocity model, especially in its deeper part. This result can be used as an initial model for the standard MVA, based on a much weaker assumption about the behavior of the residual moveouts picked in CIG. Note that the traveltime inversion engine (i.e., a tool responsible for the linear inverse problem solution) may be borrowed from already existing seismic data processing packages.

3 Robust Linear Traveltime Inversion

For the solution of a linear inverse problem, a tomographic system of linear algebraic equations (SLAE) is constructed during the ray tracing stage **4** and traveltime approximation stage **5**. SLAE forms a linear relationship between traveltime residuals dT and desired model update vector Δv:

$$dT = M\,\Delta v \tag{3}$$

Here M is a tomographic matrix with the elements representing derivatives of reflection traveltimes with respect to model parameters. Usually, the velocity model is parameterized by a 3D regular grid with constant velocity inside each voxel. Element M_{ij} of the matrix, M denotes a length of i-th reflected ray within j-th voxel. The voxels are numbered in continuous order; their number corresponds to the tomographic matrix columns. Each reflected ray corresponds to a row in the matrix M. The size of M in the isotropic case is $N_{Rays}x(N_X \cdot N_Y \cdot N_Z)$, where N_{Rays} is a number of successfully constructed reflected rays, whereas $N_X \cdot N_Y \cdot N_Z$ is the total count of points in the subsurface velocity grid. In a typical case, the number of rows significantly exceeds the number of columns. So we arrive at a classical "grid" tomography problem [3]. Below we follow an approach proposed by [4]. Instead of the original linear system (3), a pre-conditioned system is solved:

$$LMSR\Delta v' = LdT, \tag{4}$$

where L is a diagonal weighting matrix of rows, R is a diagonal weighting matrix of columns. S is a spatial smoother (which acts as a 3D convolution with a triangle function). Pre-conditioned system (4) is solved using the Iterative Reweighted Least-Squares (IRLS) method [24] with the norm $l_{1.5}$. The cost function which is minimized during the solution of the inverse problem may be expressed as

$$F = \|LMSR\Delta v^{'} - LdT\|_{1.5}^{1.5} + \lambda^2 \|\Delta v^{'}\|_2^2 = \|A\overrightarrow{x} - \overrightarrow{b}\|_{1.5}^{1.5} + \lambda^2 \|\overrightarrow{x}\|_2^2 \quad (5)$$

Where notations $A = LMSR$, $\overrightarrow{x} = \Delta v^{'}$, $\overrightarrow{b} = LdT$ are used.

The inverse problem comes down to solving the set of typical least-squares problems with a recursively updated matrix of weights

$$A^T W_{k-1} A\overrightarrow{x_k} = A^T W_{k-1} \overrightarrow{b} \quad (6)$$

Here diagonal weighting matrix W_k at k-th IRLS iteration is determined as $W_k = diag|r_i|^{-0.5}$, where $r_i = \sum A_{ij} - b_i$ is a residual vector after *(k-1)*-th iteration. SLAE's (6) is solved using the LSQR method [25]. The solution of the system (4) with the help of IRLS allows us to obtain solutions that are much more stable to abrupt "jumps" of input data (outliers). Outliers' impact on the final solution is a significant challenge in tomographic problems using the standard least-squares method.

It is important to highlight key features of SLAE's arising in seismic tomography that is important for the chosen realization of the code: 1) Huge dimensions of the system of equations ($> 10^6$ equations with more than 10^8 unknowns); 2) Matrix is very sparse with a relatively small number of nonzero elements (~1–3%); 3) Problem is ill-posed demanding usage of pre-conditioning and regularization procedures. For real-world applications, gigabytes of memory are needed to operate with such matrices (even taken into account their sparsity). Software implementation of 3D tomography should be initially focused on using high-performance computing systems with distributed memory (MPI - implementation). Our tomography implementation is based on using the functionality contained in the freeware library PETSc (http://www.mcs.anl.gov/petsc). The PETSc library is oriented explicitly for coding MPI-oriented programs that extensively use elements of linear algebra. PETSc has the following advantages: 1) It contains a set of MPI-oriented iterative algorithms for solving SLAE such as LSQR; 2) It is suitable for working with data arrays distributed over computing nodes (matrices, vectors) and performing any operations with such objects; 3) It provides a convenient way to deal with sparse matrices and vectors distributed over cluster nodes.

Following [4], the model updates pre-conditioning based on triangular smoothing has been implemented. Smoothing is implemented as a 3D spatial convolution with triangular functions. There are two possible strategies for smoothing.

The first strategy is "multiscale" smoothing. For each linear inverse problem, we attempt to resolve many scales progressing from large to small using a fixed framework of a single linear inverse problem. Then we apply similar "multiscale" smoothing inside all other linear iterations. Let's describe the main concept of the multiscale approach briefly. Initial problem (4) is represented as a series of the problems with "k" smoother S scales,

$$\sum_{k=1}^{N_S} [LMS_k R]\Delta v_{k-1} = d \quad (7)$$

At the first "multiscale" iteration, $k = 1$, one fixes the biggest smoother apertures and solve the system using the IRLS method:

$$[LMS_1R]\Delta v_1 = d \tag{8}$$

When the "long-wavelength" solution $\hat{v}_1$ is obtained, the smoother aperture is decreased, and the linear system at the next scale is solved:

$$[LMS_2R]\Delta v_2 = d - [LMS_1R]\Delta\widehat{v_1} = d_2. \tag{9}$$

This stage is repeated for each given smoother scale. Note that event positions remain fixed within the current velocity model, i.e., tomographic matrix M is the same during all iterations with different smoother apertures.

This classical "multiscale" approach is proven efficient in MVA applications [4]. The remigration stage is very computationally expensive. 3D PSDM and RMO picking have to be redone for each updated velocity model.

The second strategy is "individual" smoothing for each linear inverse problem. We resolve only a specific scale of velocity variation within one solution of a single linear inverse problem. At the same time, smoothing aperture can vary for other linear iterations. The second approach consists of solving the system (8) with a fixed "individual" smoothing aperture at each linear iteration. In this case, matrix M is recalculated once again after each iteration, and we apply a new smoother aperture. In this case number of smothers, apertures equal the number of nonlinear iterations.

For our approach, where the remigration stage is relatively cheap, the second approach is the most efficient way to solve the problem. Of course, the multiscale approach may also be used. We implemented the multiscale approach and used it in all examples in this paper.

4 Real Data Numerical Example

The approach described above was applied for depth-velocity model building for a certain area located in the Kara Sea. A narrow azimuth marine survey was performed for this area. The maximum offset in the data is 3800 m. Sea depth doesn't exceed 250 m in the acquisition area. A fragment of the investigated area 40 × 10 km (inline/crossline) has been selected. Thus, the size of the area selected for the numerical test was equal to 400 km^2. The eight most significant reflection horizons were picked in the final PSTM cube. Tables specifying the dependence $T^j_{IM}(X_{IM}, Y_{IM})$ for each horizon were provided with a spatial step of 25 × 12.5 m, which corresponds to a 3D seismic survey's binning size. An example of 4 surfaces (of a total of 8) is presented in Fig. 4. The initial velocity model (shown in Fig. 5) was obtained by the standard method by converting time migration velocities to interval velocities according to the Dix formula. Discretization of the model is 25 × 12.5 × 10 m (inline, crossline, depth). The total depth of the model is 7 km. Traveltime inversion was performed using a coarser grid 100 × 100 × 50 m. The. The smoothers width in operator S decreased using four consecutive steps during global iterations of model refinement: initial widest smoothers are 3000 × 3000 × 1000 m, the final widths are ten times smaller, i.e., 300 × 300 × 100 m. It allows moving gradually

from long-wavelength velocity variations to more detailed ones avoiding manifestation of instability. The total number of global nonlinear iteration was 12. While solving SLAE, the number of LSQR iteration was 20, whereas the number of IRLS (outer) iterations was equal to 10. Apertures for local reflection surface approximation (stage 2 of the proposed workflow) were chosen as 100 × 100 m (inline/crossline).

The recovered depth velocity model is presented in Fig. 6. The PSDM results using the initial velocity model are presented in Figs. 7a and 8a. As one can see from the CIG gathers (see Fig. 7a, where a fragment taken along the inline direction from the center of the 3D model is presented), the initial depth velocity model is far from satisfactory. At the bottom part of the images coherent events are not visible at all. It would make the use of standard MVA very difficult. In the stacked PSDM image (Fig. 8a), one can observe defocusing and poor coherency along the main reflection horizons. PSDM performed using a recovered depth velocity model (Fig. 6) allows obtaining very satisfactory results (Fig. 7b and 8b).

The results presented in this section prove the efficiency of the proposed approach. In the cases where the hyperbolic reflection traveltime approximation describes the real reflection arrivals in a sufficiently far range of offsets, the proposed algorithm could replace the standard MVA. Recall, though, that its main purpose is to be used before the standard MVA is applied to provide a reliable initial depth velocity model, which may be refined with minimum MVA iterations.

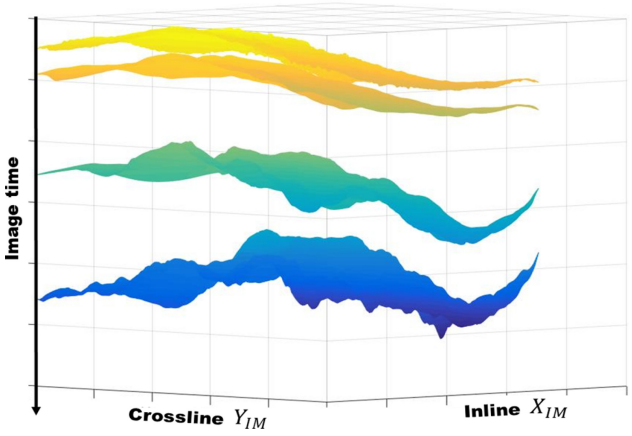

Fig. 4. Time migrated surfaces picked in PSTM cube.

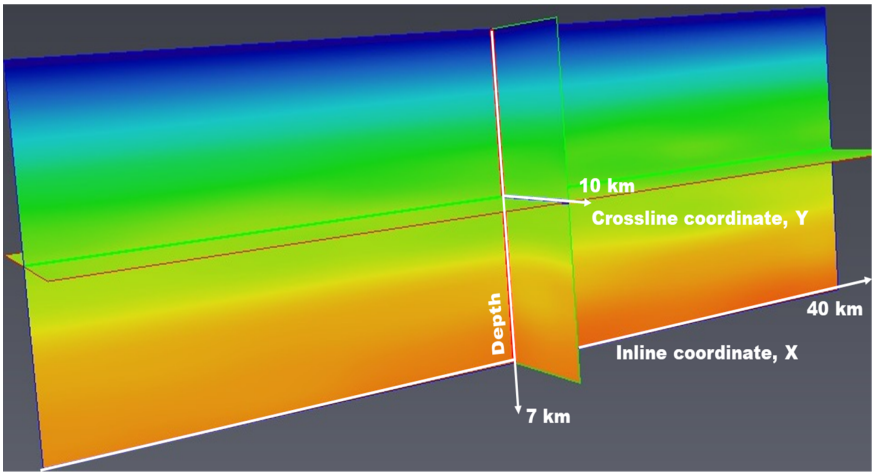

Fig. 5. Initial depth velocity model; model size is 40 × 10 × 7 km (X,Y,Z); velocity variations are within the range [1500–4400] m/s.

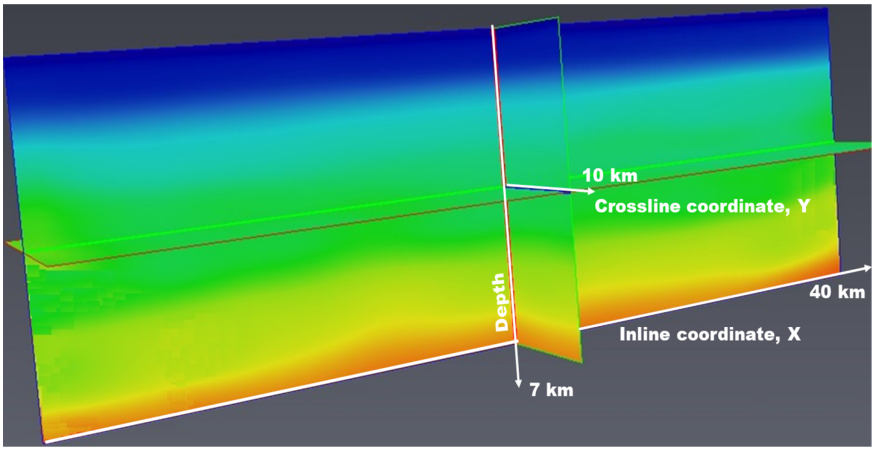

Fig. 6. Recovered depth velocity model using the proposed approach; velocity variations are within the range [1500–4400] m/s.

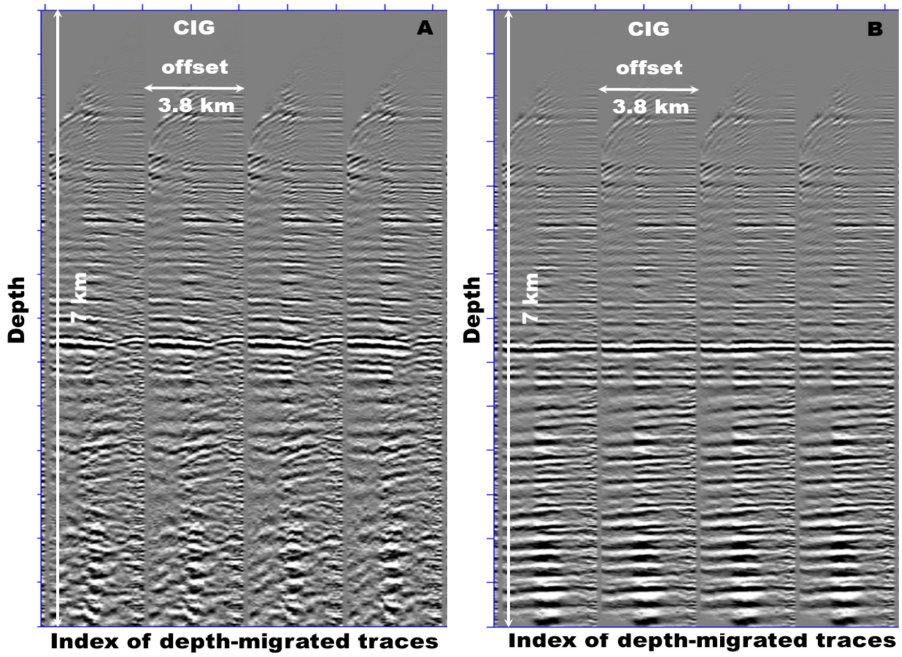

Fig. 7. Common-image gathers obtained by PSDM using (a) initial depth-velocity model; (b) recovered depth-velocity model.

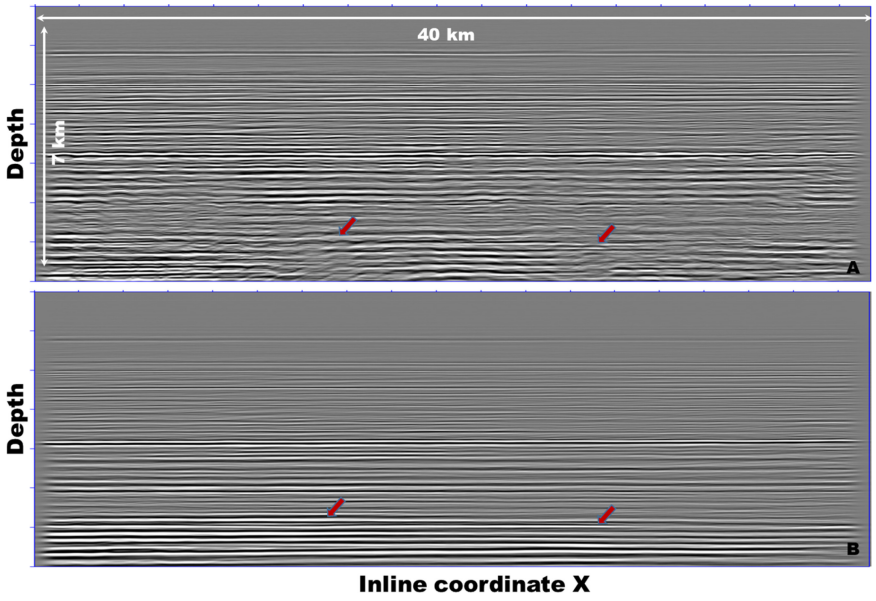

Fig. 8. Final PSDM images obtained using a) initial velocity model, b) recovered velocity model. The inline section from the middle of the models is presented.

5 Conclusions

We presented a robust nonlinear 3D reflection traveltime tomography workflow based on the use of time processing products such as NMO velocity and picked time-migrated horizons. Picking is performed within the resulting PSTM image. After numerical demigration of time-migrated surfaces, we utilized hyperbolic reflection traveltime approximation directly in the data domain. We did it instead of picking reflection traveltimes in the image domain like in standard MVA. The proposed approach enables fast iterative depth velocity model reconstruction. The reliability of the recovered model is limited due to the approximation of real reflection traveltimes, but such a model could serve as an initial velocity model for MVA. The use of an advanced initial model allows reducing the number of computationally expensive MVA iterations.

In some cases, where the hyperbolic reflection traveltime approximation can describe the real reflection arrivals in a sufficiently far range of offsets, the proposed algorithm could replace the standard MVA. The advantages of the proposed algorithm are the following: 1) there is no need for preliminary manual interpretation of seismic volumes since the algorithm is fully automatic and based on grid reflection tomography, 2) there is no need for computationally expensive two-point or dynamic raytracing, and 3) it is much cheaper computationally than standard common-image point tomography in the image domain. Real data examples confirm that depth images using the velocity model recovered by the proposed approach are more focused, and the flattening of the corresponding common-image gathers was improved.

Acknowledgments. The reported study was funded by RFBR, project number 20–55-26003, and by the Czech Science Foundation under contract 21-15272J.

References

1. Fagin, S.: Model Based Depth Imaging. SEG (1999)
2. Robein, E.: Seismic Imaging: A Review of the Techniques, their Principles, Merits and Limitations. EAGE (2010)
3. Jones I.F.: An Introduction to: Velocity model Building. EAGE (2010)
4. Woodward, V., Nichols, D., Zdraveva, O., Whitfield, P., Johns, T.: A decade of tomography. Geophysics **73**, VE5-VE11 (2008)
5. Cameron, M., Fomel, S., Sethian, J.: Time-to-depth conversion and seismic velocity estimation using time-migration velocity. Geophysics **73**, VE205-VE210 (2008)
6. Iversen, E., Tygel, M.: Image-ray tracing for joint 3D seismic velocity estimation and time-to-depth conversion. Geophysics **73**, S99–S114 (2008)
7. Santos H.B., Schleicher J., Novais A.: Initial-model construction for MVA techniques. In: Proceedings of the 2013 75th EAGE Conference and Exhibition, EAGE (2013)
8. Dell, S., Gajewski, D., Tygel, M.: Image-ray tomography. Geophys. Prospect. **62**, 413–426 (2014)
9. Lambare, G., Guillaume, P., Montel, J.P.: Recent advances in ray-based tomography. In: Proceedings of 2014 76th EAGE Conference and Exhibition, EAGE (2014)
10. Li, S., Fomel, S.: A robust approach to time-to-depth conversion and interval velocity estimation from time migration in the presence of lateral velocity variations. Geophys. Prospect. **63**, 315–337 (2015)

11. Santos, H.-B., Schleicher, J., Novais, A., Kurzmann, A., Bohlen, T.: Robust time-domain migration velocity analysis for initial-model building in a full-waveform tomography workflow. In: Proceedings of 2016 87th SEG Annual Meeting, pp. 5307–5312. SEG (2016)
12. Sadala Valente, L.S., Santos, H., Costa, J., Schleicher, J.: Time-to-depth conversion and velocity estimation by image-wavefront propagation. Geophysics **82**, U75–U85 (2017)
13. Sripanich, Y., Fomel, S.: Fast time-to-depth conversion and interval velocity estimation in the case of weak lateral variations. Geophysics **83**, S227–S235 (2018)
14. Zhao, H., Ueland Waldeland, A., Rueda Serrano, D., Tygel, M., Iversen, E.: Time-migration tomography based on reflection slopes in pre-stack time-migrated seismic data. In: Proceedings of 2018 80th EAGE EAGE Conference and Exhibition. EAGE (2018)
15. Duveneck, E.: Velocity model estimation with data-derived wavefront attributes. Geophysics **69**, 265–274 (2004)
16. Lambaré G.: Stereotomography. Geophysics, 73, VE25-VE34 (2008)
17. Gelius, L.-J., Tygel, M.: Migration-velocity building in time and depth from 3D (2D) Common-Reflection-Surface (CRS) stacking - theoretical framework. Stud. Geophys. Geod. **59**(2), 253–282 (2015). https://doi.org/10.1007/s11200-014-1036-6
18. Mesquita, L., Jorge, M., Cruz, R., Callapino, J.C., Garabito, G.: Velocity inversion by global optimization using finite-offset common-reflection-surface stacking applied to synthetic and Tacutu Basin seismic data. Geophysics **84**, R165–R174 (2019)
19. Dix, C.H.: Seismic velocities from surface measurements. Geophysics **20**, 68–86 (1955)
20. Hubral, P., Krey, T.: Interval velocities from seismic reflection time measurements. SEG (1980)
21. Yilmaz, O.: Seismic Data Analysis: Processing, Inversion, and Interpretation of Seismic Data. SEG (2001)
22. Gjoystdal, H., Ursin, B.: Inversion of reflection times in three dimensions. Geophysics **46**, 972–983 (1981)
23. Al-Chalabi, M.: Series approximation in velocity and traveltime computations. Geophys. Prosp. **21**, 783–795 (1973)
24. Alkhalifah, T.: Velocity analysis using nonhyperbolic moveout in transversely isotropic media. Geophysics **62**, 1839–1854 (1997)
25. Scales, J., Gersztenkorn, A., Treitel, S.: Fast Lp solution of large, sparse linear systems, application to seismic traveltime tomography. J. Compu. Phys. **75**, 313–333 (1988)
26. Paige, C.C., Saunders, M.A.: LSQR: an algorithm for sparse linear equations and sparse least squares. ACM Trans. Math. Softw. **8**(1), 43–71 (1982)